

PAPER

# Parametric study of linear stability of toroidal Alfvén eigenmode in JET and KSTAR

To cite this article: J. Seo *et al* 2020 *Nucl. Fusion* **60** 066008

View the [article online](#) for updates and enhancements.



**IOP | ebooks™**

Bringing together innovative digital publishing with leading authors from the global scientific community.

Start exploring the collection—download the first chapter of every title for free.

# Parametric study of linear stability of toroidal Alfvén eigenmode in JET and KSTAR

J. Seo<sup>1</sup> , J. Kim<sup>2</sup> , J. Mailloux<sup>3</sup>, R.J. Dumont<sup>4</sup> , M. Fitzgerald<sup>3</sup>, S.E. Sharapov<sup>3</sup>, D.L. Keeling<sup>3</sup>, F. Koechl<sup>3</sup>, F.J. Casson<sup>3</sup> , C.Y. Lee<sup>1</sup>, T.S. Hahm<sup>1</sup>, Y.-S. Na<sup>1</sup> and JET contributors<sup>a</sup>

<sup>1</sup> Department of Nuclear Engineering, Seoul National University, Seoul, Korea, Republic Of

<sup>2</sup> National Fusion Research Institute, Daejeon, Korea, Republic Of

<sup>3</sup> Culham Science Centre, Culham Centre for Fusion Energy, Abingdon OX14 3DB, United Kingdom of Great Britain and Northern Ireland

<sup>4</sup> CEA, IRFM, F-13108 Saint-Paul-les-Durance, France

E-mail: [ysna@snu.ac.kr](mailto:ysna@snu.ac.kr)

Received 15 December 2019, revised 11 March 2020

Accepted for publication 13 March 2020

Published 28 April 2020



CrossMark

## Abstract

Parametric dependencies of the linear stability of toroidal Alfvén eigenmode (TAE) in the presence of neutral beam injection (NBI) are investigated to understand the beam drive and damping effect of TAEs in JET and KSTAR. It is found that the results depend on the drift orbit width of the beam-ions normalized to the characteristic mode widths. In addition, an analytic expression of the linear growth rate of TAE driven by ion cyclotron resonance heating (ICRH) fast ions is derived. The developed model is applied to the linear stability analysis of a time-varying JET discharge where both the beam damping and the drive are observed with NBI and ICRH. It can successfully reproduce the experimental observations in spite of simple approximations such as the slowing-down distribution for beam-ions and bi-Maxwellian for ICRH fast ions. We note that strong interaction of TAE with beam occurs in plasmas with rather high density with  $n_l \gtrsim B_0^2/9 \mu_0 M_i v_0^2$  favorable for the resonance condition,  $v_0 > v_A/3$ . The developed model can allow fast estimation of the linear stability of TAEs, so it should be useful for optimizing the scenarios and feedback control.

Keywords: tokamak, energetic particle, toroidal Alfvén eigenmode, JET, KSTAR

(Some figures may appear in colour only in the online journal)

## 1. Introduction

Many energetic ions such as alpha particles from the fusion reaction of deuterium–tritium (DT) plasmas as well as those generated by auxiliary heating, neutral beam injection (NBI) and ion cyclotron resonance heating (ICRH) can be present in magnetic confinement fusion devices such as tokamak. In ITER, a 1 MeV NBI system is supposed to be installed, and the 3.5 MeV alpha particles will be produced from the DT fusion

reaction, resulting in generation of plentiful super-Alfvénic ions.

Toroidal Alfvén eigenmodes (TAEs) are discrete modes in the gap structure generated by the mode coupling of poloidally adjacent shear Alfvénic modes in toroidal geometry which are weakly damped in the absence of energetic ions [1, 2]. Super-Alfvénic ions mentioned above can be a free energy source which destabilize TAEs with a wave–particle interaction [3]. This interaction between energetic ions and shear Alfvén waves inevitably leads to the radial transport of resonant energetic ions, potentially resulting in a significant wall damage and degradation of the performance of plasmas. The

<sup>a</sup> See Joffrin *et al* 2019 (<https://doi.org/10.1088/1741-4326/ab2276>) for the JET team.

observations of the fast ion losses due to the Alfvénic activity have been reported in various devices such as DIII-D [4], TFTR [5], JET [6, 7], ASDEX-U [6, 8] and KSTAR [9, 10]. Therefore, it is essential to understand the physics of stability of AEs in a tokamak with a high content of energetic ions such as in JET DT discharges and ITER.

In various present tokamaks, it has usually been observed that beam-ions born by NBI induce the TAEs. On the contrary, in TFTR [11] and JET [12], it was found that the beam-ions damp TAEs (driven by other mechanisms, not NBI) even with the negative gradient of the beam pressure which is known to be the free-energy source of the modes. Therefore, it is important to find out under what conditions, the beam can drive or damp TAEs for the prediction of the effect of NBI on the mode stability in future tokamaks. Analytic estimation of the energetic ions' effect on TAE stability was first carried out by Fu and Van Dam [13], by deriving the interaction between TAE and alpha particles from the linearized drift kinetic equation. Later, the finite orbit width (FOW) effects for various orbit width regimes were revealed which have the stabilizing effect of TAE drive and different dependence of the mode number [14–16]. Although these analytic theories adopted simple assumptions, they provide us physics insight to figure out the parametric dependence of the linear stability of TAE without relatively time-consuming MHD or gyrokinetic codes.

In this study, we use these analytic expressions of the linear growth rate of TAEs to analyze the parametric dependence of the mode stability in the presence of beam-ions and for application to stability analysis of TAEs in a JET discharge. In section 2, we describe a set of the formulas of the linear growth rate of TAEs, including new modeling of the ICRH fast ion interaction with modes for JET application. Parametric dependence of the beam-ion property on their interaction with TAEs is discussed in section 3. In section 4, we will apply the analytic formulas to a time-evolving JET plasma. In addition, the contribution of alpha particles to TAEs in JET DT plasmas is predicted in section 5. Finally, conclusions will be drawn in section 6.

## 2. Interaction of TAE with particles

The stability of the modes is quantified by the linear growth rate,  $\gamma$ , which can be expressed by a summation of all contributions of the interacting species, in the following form,

$$\frac{\gamma}{\omega} \simeq \left(\frac{\gamma}{\omega}\right)_{\alpha} + \left(\frac{\gamma}{\omega}\right)_{NB} + \left(\frac{\gamma}{\omega}\right)_{RF} + \left(\frac{\gamma}{\omega}\right)_i + \left(\frac{\gamma}{\omega}\right)_e, \quad (1)$$

where  $\omega$  is the real frequency. The terms in the right-hand side are the linear growth rate by fusion alpha particles, beam-ions from NBI, fast ions from ICRH, bulk ions, and electrons, respectively. Here, we focus on the flat and broad gap structure to study the TAE interaction with particles only, so the continuum damping [17, 18] and the radiative damping [19] are not considered.

With the expressions derived from the analytic theories for each term in equation (1), we can check the linear stability of TAEs without consuming lots of computational loads by

using MHD or gyrokinetic codes to estimate the mode stability. For this reason, this method using the analytic formulas has been used for predicting the mode stability in the global region with diverse conditions in ITER [20, 21] or analyzing the time-evolution of the quasilinear interaction of energetic ions with TAE in time-varying heating and transport situations [22]. However, most of studies consider the mode drive only by the energetic ions, without considering the damping contribution by them. In this study, we consider both the mode drive and damping by energetic ions to describe the TAEs disappearing by NBI in JET, and model the ICRH fast ion interaction with the modes for the ICRH-driven TAEs.

### 2.1. Interaction of TAE with NBI or alpha particles

Beam-ions from NBI or alpha particles from DT fusion reactions can interact with TAEs at the resonant velocity,  $v_{\parallel} = v_A/|2s-1|$ , where  $v_{\parallel}$  is the parallel velocity of the particle,  $v_A$  the Alfvén velocity, and  $s = 0, \pm 1, \pm 2, \dots$  the integer resonance number. It is important to notice that the theory of this wave-particle interaction varies greatly depending on a key dimensionless parameter  $\Delta_b/\Delta_m^{(o)}$  which determines different radial structures of the mode. Here,  $\Delta_b \simeq qv_{\parallel}/\omega_c$  (for passing particle) is the drift orbit width of energetic ions with  $q$  the safety factor and  $\omega_c$  the cyclotron frequency.  $\Delta_m^{(o)} = r/m \simeq r/nq$  is the outer mode width with  $r$  the location of the mode in minor radius,  $m$  the poloidal mode number, and  $n$  the toroidal mode number. The drive and the damping rate of TAE by beam-ions can be expressed as [16]

$$\left(\frac{\gamma}{\omega}\right)_{NB}^{drive} = -q^2 \beta_b \frac{\omega_{*b}}{\omega} (1 + \cos^2 \theta_0)^2 \sum_s C_{ow,s}^{NB} \quad (2)$$

and

$$\left(\frac{\gamma}{\omega}\right)_{NB}^{damp} = -3q^2 \beta_b (1 + \cos^2 \theta_0)^2 \sum_s \frac{C_{ow,s}^{NB}}{y_s^2} \quad (3)$$

where

$$C_{ow,s}^{NB} = \begin{cases} \frac{3\pi}{4} y_s^4 \eta (1 - y_s) & \Delta_b \ll \Delta_m^{(i)} \\ \frac{4\Delta_m^{(i)}}{\zeta_p} y_s^3 \eta (1 - y_s) & \Delta_m^{(i)} \ll \Delta_b \ll \Delta_m^{(o)} \\ \frac{24\Delta_m^{(i)} \Delta_m^{(o)2}}{\zeta_p^3} y_s \eta (1 - y_s) & \Delta_b \gg \Delta_m^{(o)} \end{cases} \quad (4)$$

is the coefficient including the orbit width effect which varies with the beam-ion orbit width.  $\beta_b = \frac{P_b}{B_0^2/2\mu_0}$  is the toroidal beta of the beam-ions with  $P_b$  beam pressure,  $B_0$  the toroidal magnetic field, and  $\mu_0$  the vacuum permeability.  $\omega_{*b} = \frac{nqv_0^2}{r\omega_c} \frac{\partial \ln \beta_b}{\partial r}$  is the diamagnetic frequency of the beam-ions,  $\cos \theta = v_{\parallel}/v$  is the pitch angle variable of the beam-ions,  $\cos \theta_0$  is the birth pitch angle,  $y_s = v_A/|2s-1|v_0 \cos \theta_0$  is the resonance parameter with  $v_0$  birth beam velocity,  $\eta(x)$  is Heaviside step function,  $\Delta_m^{(i)} = \frac{5\pi}{16} \frac{r^2}{mR_0} \left(\simeq \Delta_m^{(o)}\right)$  is the inner mode width with  $R_0$  the major radius at the magnetic axis,  $\simeq = r/R_0$ , and  $\zeta_p = (1 + \cos^2 \theta_0) qv_0/(\omega_c \cos \theta_0)$ . Here, beam-ion distribution is assumed as a strongly anisotropic slowing-down distribution,  $f_0 = \frac{3\beta_b B_0^2}{2\pi\mu_0 M_b v_0^2} \frac{\eta(v_0 - v)}{v^3} \delta(\cos \theta - \cos \theta_0)$ .

For passing alpha particles with the isotropic slowing-down distribution ( $f_0 = A \frac{\eta(v_0 - v)}{v^3}$ ), we can express the drive and the damping term as in [16]

$$\left(\frac{\gamma}{\omega}\right)_{\alpha}^{drive} = -q^2 \beta_{\alpha} \frac{\omega_{* \alpha}}{\omega} \sum_s C_{ow,s}^{\alpha} y_s (1 + 6y_s^2 - 4y_s^3 - 3y_s^4) \quad (5)$$

and

$$\left(\frac{\gamma}{\omega}\right)_{\alpha}^{damp} = -3q^2 \beta_{\alpha} \sum_s C_{ow,s}^{\alpha} y_s (3 + 4y_s - 6y_s^2 - y_s^4) \quad (6)$$

where

$$C_{ow,s}^{\alpha} = \begin{cases} \frac{\pi}{16} \eta (1 - y_s) & \Delta_b \ll \Delta_m^{(i)} \\ \frac{\Delta_m^{(i)}}{3\Delta_{b0}} \eta (1 - y_s) & \Delta_m^{(i)} \ll \Delta_b \ll \Delta_m^{(o)} \\ \frac{\Delta_m^{(o)} (\Delta_m^{(o)})^2}{2\Delta_{b0}^3} \eta (1 - y_s) & \Delta_b \gg \Delta_m^{(o)} \end{cases} \quad (7)$$

is the coefficient for the linear growth rate by alpha particles including the orbit width effect.  $\beta_{\alpha} = \frac{P_{\alpha}}{B_0^2/2\mu_0}$  is the toroidal beta of the alpha particles with  $P_{\alpha}$  the alpha pressure,  $\omega_{* \alpha} = \frac{nqv_{\alpha}^2}{r\omega_c} \frac{\partial \ln \beta_{\alpha}}{\partial r}$  is the diamagnetic frequency,  $y_s = v_A/(2s-1)v_{\alpha}$  is the resonance layer parameter with  $v_{\alpha}$  the alpha birth velocity, and  $\Delta_{b0} = qv_{\alpha}/\omega_c$  is the alpha orbit width at the birth velocity.

Here, we note that the expressions for alpha particles are valid for  $y_s > \sqrt{2}\epsilon$ , and become identical with those in [23] for the zero orbit width (ZOW) limit ( $\Delta_b \ll \Delta_m^{(i)}$ ). As the normalized fast ion orbit width  $x_{ow} \equiv \Delta_b/\Delta_m^{(o)}$  increases, the coefficients of the linear growth rate, (4) and (7) become significantly reduced by a scale of  $1/x_{ow}$  in  $\epsilon \ll x_{ow} \ll 1$  and  $1/x_{ow}^3$  in  $x_{ow} \gg 1$ . This scaling indicates that the TAE interactions with energetic ions including both the drive and the damping effect become smaller in the large-orbit width regime. Furthermore, since  $\frac{drive}{damping} \sim \frac{\omega_{*}}{\omega} \propto \frac{\Delta_b}{\Delta_m}$  [14], the fast ion orbit width determines the role of the resonant ions (driving or damping) on the mode, which will be discussed in detail in section 3.

## 2.2. Interaction of TAE with ICRH fast ions

In JET, TAEs are usually driven by ICRH fast ions, showing different properties from NBI-driven modes in other devices. ICRH fast ions are strongly anisotropic with  $T_{\perp} > T_{\parallel}$ , so their resonance mechanism with TAE is quite different from passing particles like beam-ions. The TAE resonance condition for trapped ions is

$$\omega - s\omega_b - n\omega_D = 0 \quad (8)$$

where  $\omega_b$  is the bounce frequency and  $\omega_D$  is the precessional drift frequency of the trapped particles.  $s$  is the resonance harmonic number mentioned in section 2.1 and  $n$  is the toroidal mode number. This condition determines the resonance velocity condition for trapped particles,  $v = v_1 \equiv -\sqrt{\frac{\epsilon}{2} \frac{r\omega_c}{n^2 q^2}} +$

$$\sqrt{\left(\sqrt{\frac{\epsilon}{2} \frac{r\omega_c}{n^2 q^2}}\right)^2 + \frac{r\omega_c v_A}{n^2 q^2}} \quad [16].$$

Since the drift orbit width of the well trapped resonant ion,  $\Delta_{b,t|res} \simeq 2\sqrt{2}qv_1/\sqrt{\epsilon}\omega_c$ , is much greater than that of

the passing ion, it is relatively easy to exceed the outer mode width,  $\Delta_m^{(o)}$ . For the typical values of ICRH fast ions in JET and ITER, one can check that  $\Delta_{b,t}/\Delta_m^{(o)} \sim 10$ , so we should adopt the nonlocal theory for the  $\Delta_b \gg \Delta_m^{(o)}$  regime. In this regime, the linear growth rate of TAE by the trapped ions can be obtained from [16]

$$\frac{\gamma}{\omega} \simeq \frac{256\pi\mu_0\sqrt{2}\epsilon q^3 n M_f v_1^6}{B_0^2 r \omega_c D_1} J_0^2\left(\frac{mv_1}{r\omega_c}\right) \int_0^{\kappa_{max}^2} \kappa^2 d\kappa^2 \frac{\Delta_m^{(i)} \Delta_m^{(o)2}}{\Delta_{b,t}^3} \left(\frac{\omega}{\omega_*} - 1\right) \frac{\partial f_0}{\partial r} \Big|_{v=v_1} \quad (9)$$

with  $M_f$  the mass of the resonant ions,  $J_0(x)$  the 0th-order Bessel function of the first kind,  $\kappa$  the trapping parameter ( $\kappa^2 < 1$  for trapping),  $\Delta_{b,t} = 2\sqrt{2}q\kappa v/\sqrt{\epsilon}\omega_c$  the orbit width of the trapped ions,  $f_0$  the distribution function of the fast ions,  $\omega_* = \frac{nqv}{\omega_c r} \frac{\partial f_0/\partial r}{\partial f_0/\partial v}$ , and  $D_1 = \frac{nqv_1}{rR_0\omega_c} + \frac{1}{qR_0} \sqrt{\frac{\epsilon}{2}}$ . Here, the term of the radial gradient of the distribution  $\frac{\partial f_0}{\partial r}$  is a driving source while  $\frac{\omega}{\omega_*} \frac{\partial f_0}{\partial r} \propto \frac{\partial f_0}{\partial v}$  is a damping source.

If we determine the distribution function of the trapped fast ions, the linear growth rate from their wave-particle interaction can be calculated. To model the ICRH-driven TAE, we assume the distribution function for the ICRH fast ions as a bi-Maxwellian with  $T_{\perp} > T_{\parallel}$ ,

$$f_0 = \frac{n_f}{T_{\perp}\sqrt{T_{\parallel}}} \left(\frac{M_f}{2\pi}\right)^{\frac{3}{2}} \exp\left[-\frac{M_f v_{\parallel}^2}{2T_{\parallel}}\right] \exp\left[-\frac{M_f v_{\perp}^2}{2T_{\perp}}\right] \quad (10)$$

where  $n_f$  is the ICRH fast-ion density,  $T_{\parallel}$  and  $T_{\perp}$  are the parallel and the perpendicular temperature of the fast ions, respectively. It is more realistic to use a distribution function presented in [24] which includes a property of the accumulation of banana tips of the fast ions in the cyclotron resonance layer. In this study, however, we adopted bi-Maxwellian expressed with variables that can be obtained by ICRH modeling codes to make it analytically integrable the integrand in equation (9). For more sophisticated estimation, it is required to calculate numerical integration using another distribution form. Substituting the distribution function (10) into (9) we obtain the TAE drive and the damping rate by ICRH fast ions for the  $\Delta_b \gg \Delta_m^{(o)}$  regime,

$$\left(\frac{\gamma}{\omega}\right)_{RF}^{drive} = -nq^3 \frac{\partial \beta_f}{\partial r} J_0^2\left(\frac{mv_1}{r\omega_c}\right) \frac{\Delta_m^{(i)} \Delta_m^{(o)2}}{\zeta_i^3} \frac{v_1}{D_1 r \omega_c} F_{rf}\left(\frac{v_{\perp}}{v_{T\perp}}, \frac{v_{\parallel}}{v_{T\parallel}}\right) \quad (11)$$

and

$$\left(\frac{\gamma}{\omega}\right)_{RF}^{damp} = -q\beta_f J_0^2\left(\frac{mv_1}{r\omega_c}\right) \frac{\Delta_m^{(i)} \Delta_m^{(o)2}}{\zeta_i^3} \frac{\sqrt{\epsilon} v_A}{D_1 R_0 v_1} G_{rf}\left(\frac{v_{\perp}}{v_{T\perp}}, \frac{v_{\parallel}}{v_{T\parallel}}\right) \quad (12)$$

with  $\zeta_i = 2\sqrt{2}qv_1/\sqrt{\epsilon}\omega_c$ ,  $v_{T\parallel,\perp} = \sqrt{T_{\parallel,\perp}/M_f}$ ,  $F_{rf}(x_{\perp}, x_{\parallel}) = \frac{96x_{\parallel}x_{\perp}^4}{\sqrt{x_{\parallel}^2 - x_{\perp}^2}} e^{-x_{\perp}^2/2} \text{erf}\left\{\sqrt{\epsilon}\left(x_{\parallel}^2 - x_{\perp}^2\right)\right\}$ , and  $G_{rf}(x_{\perp}, x_{\parallel}) = 48x_{\parallel}x_{\perp}^4 e^{-\frac{x_{\perp}^2}{2}} \left[\frac{(1+x_{\perp}^2) \text{erf}\left\{\sqrt{\epsilon}\left(x_{\parallel}^2 - x_{\perp}^2\right)\right\}}{\sqrt{\epsilon}\left(x_{\parallel}^2 - x_{\perp}^2\right)} - \frac{2}{\sqrt{\pi}} e^{-\epsilon\left(x_{\parallel}^2 - x_{\perp}^2\right)}\right]$

for  $x_{\perp} = v_{\perp}/v_{T\perp}$  and  $x_{\parallel} = v_{\parallel}/v_{T\parallel}$ .  $\beta_f = \frac{n_f T_f}{B_0^2/2\mu_0}$  is the toroidal

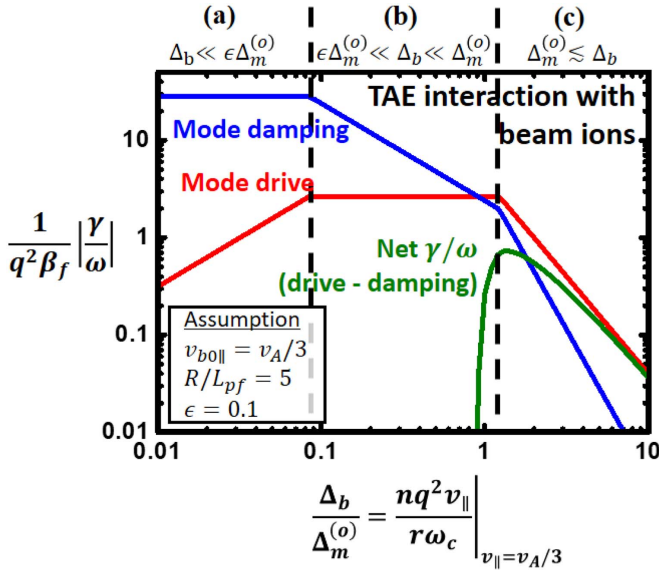


**Figure 1.** TAE drive and damping rates by beam-ions (sideband resonance) with beam-ion orbit width. The  $x$ -axis corresponds to the normalized beam-ion orbit width and the  $y$ -axis to the normalized value of the linear growth rate. Asymptotic dependences of the drive (red line) and the damping (blue line) of TAE by beam-ions in  $\Delta_b \ll \Delta_m^{(o)}$  (a),  $\epsilon \Delta_m^{(o)} \ll \Delta_b \ll \Delta_m^{(o)}$  (b), and  $\Delta_m^{(o)} \lesssim \Delta_b$  (c) regimes are shown. The green line is the resulting net growth rate (drive-damping). Beam-drive is dominant for  $\Delta_b/\Delta_m^{(o)} \gtrsim 1$  and beam-damping for  $\Delta_b/\Delta_m^{(o)} \lesssim 1$ .

beta of ICRH fast ions with  $T_f = \frac{1}{3}(T_{\parallel} + 2T_{\perp}) \simeq \frac{2}{3}T_{\perp}$  for  $2T_{\perp} \gg T_{\parallel}$ .

For the case that the orders of magnitude of the dimensionless functions  $F_{rf}$  and  $G_{rf}$  are same, we see that

$$\left| \frac{\gamma_{RF}^{drive}}{\gamma_{RF}^{damp}} \right| \sim \frac{nq^2}{L_{pf}} \frac{R_0 v_{\parallel}^2}{r \omega_c \sqrt{\epsilon} v_A} \sim \frac{1}{\epsilon^{3/2}} \frac{\Delta_{b,t}}{\Delta_m^{(o)}} \gg 1 \quad (13)$$

with  $L_{pf} = \left| \frac{\beta_f}{\partial \beta_f / \partial r} \right|$  the pressure scale length for the fast ions and approximation of  $v_{\parallel} \simeq v_A / \sqrt{2\epsilon}$ . This ordering indicates that the ICRH fast ions in this regime have a role of destabilizing rather than damping TAEs, in agreement with the experimental observations in JET.

### 2.3. Dissipation of TAE in a tokamak

One of the main damping mechanisms of TAEs driven by energetic ions is Landau damping by bulk ions. The damping of TAEs by bulk ions is very sensitive to the ion temperature with exponential dependence, which can be expressed as in [23]

$$\left( \frac{\gamma}{\omega} \right)_i = -\frac{\sqrt{\pi}}{2} q^2 \beta_i x_i (1 + 2x_i^2 + 2x_i^4) e^{-x_i^2}. \quad (14)$$

Here,  $\beta_i = \frac{P_i}{B_0^2/2\mu_0}$  is the toroidal beta of the thermal ions with  $P_i$  the thermal ion pressure and  $x_i = \frac{v_A}{3\sqrt{2}T_i/M_i}$  with  $T_i$  the ion temperature and  $M_i$  the main ion mass. Landau damping by electrons is assumed to be subdominant here due to their high thermal velocities.

The collisional damping of the trapped electrons can be another effective damping mechanism [25, 26],

$$\left( \frac{\gamma}{\omega} \right)_e = -\sqrt{\frac{\nu_e}{\omega}} \left( 3.9\beta_e q^2 + 0.44 \left( \frac{\rho_s m}{r} \right)^2 \right) \left[ \ln \left( 16 \sqrt{\frac{\epsilon \omega}{\nu_e}} \right) \right]^{-3/2} \quad (15)$$

where  $\beta_e = \frac{P_e}{B_0^2/2\mu_0}$  is the toroidal beta of the electrons with  $P_e$  the electron pressure,  $\nu_e$  is the electron collisional frequency, and  $\rho_s = c_s/\omega_c$  with  $c_s$  the ion sound speed.

Continuum damping [17, 18] and radiative damping [19] of TAEs can also become significant. In this study, we focus on a favorable gap structure with a flat  $q$ -profile which minimizes those damping processes, so those mechanisms are not included in the computation. Nonlinear behaviors are also not considered which lead to the mode saturation by the change of the distribution of the energetic particles trapped in waves [27] or the interactions among the modes with different mode numbers [28–30]. These nonlinear evolutions can be important because it can destabilize linearly stable modes by mode interactions, but we only consider the linear stability here for simplicity.

### 3. The parametric criterion of beam drive/damping of TAE

As we expressed in section 2.1, energetic ions have both the effects of the drive (by  $\partial f/\partial r$ ) and the damping (by  $\partial f/\partial v$ ) of TAEs. In JET plasmas, TAEs are usually damped by beam-ions ( $\gamma_{NB}^{drive} < \gamma_{NB}^{damp}$ ) when strong NBI is injected, while they are driven by the beam-ions in other devices such as KSTAR ( $\gamma_{NB}^{drive} > \gamma_{NB}^{damp}$ ) even with the same resonance condition  $v_{\parallel} = v_A/|2s-1|$ . In this section, we try to find out which parameter plays a key role to determine the magnitude of the ratio between the mode drive and the damping by beam-ions.

The ratio of drive to damping of TAEs by energetic ions is proportional to  $\omega_{*f}/\omega$  as is well known, and it can be shown to be proportional to the normalized beam-ion orbit width,

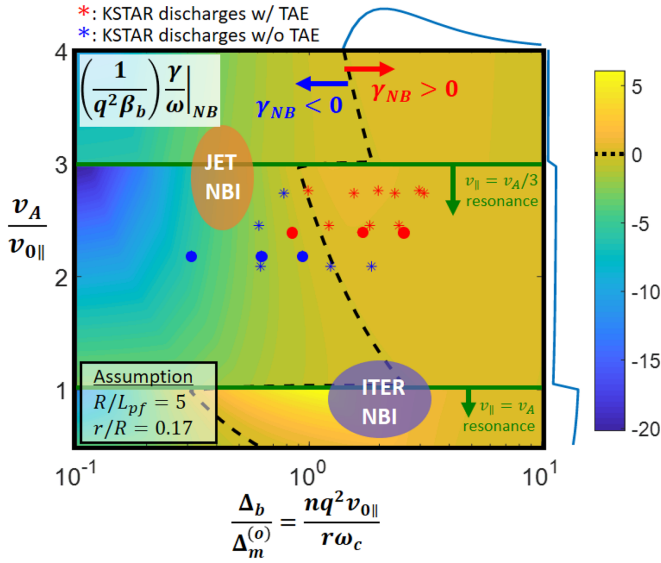
$$\left| \frac{\omega_{*f}}{\omega} \right| = \frac{1}{\omega} \left| \frac{nq v_{\parallel}}{\omega_c r} \frac{\partial f/\partial r}{\partial f/\partial v_{\parallel}} \right|_{v_{\parallel}=v_A/|2s-1|} \simeq \left( \frac{2}{3|2s-1|} \frac{R}{L_{pf}} \right) \frac{\Delta_b}{\Delta_m^{(o)}} \Big|_{v_{\parallel}=v_A/|2s-1|} \propto \frac{\Delta_b}{\Delta_m^{(o)}} \quad (16)$$

Here we assume the mode frequency at the center of the gap,  $\omega \simeq v_A/2qR$ , and  $f$  as a slowing-down distribution so that  $\frac{\partial f}{\partial v_{\parallel}} \simeq -\frac{3v_{\parallel}}{v^2} f$ . The relation (16) makes the  $\Delta_b/\Delta_m^{(o)}$ -dependence in mode drive (2) and damping rate (3) different. Therefore,  $\Delta_b/\Delta_m^{(o)}$  determines not only the finite orbit width correction term (4), but also which effect of the mode drive and damping is dominant. It is noteworthy that  $\omega_{*f}/\omega$  seems to be a more intuitive parameter for grasping the criterion to destabilize the mode due to its explicit proportion to  $\frac{\partial f/\partial r}{\partial f/\partial v_{\parallel}}$ . In this study, however, we focus on  $\Delta_b/\Delta_m^{(o)}$  instead because the governing theories also differ by their valid regime of  $\Delta_b/\Delta_m^{(o)}$  so it provides consistency and clarity in parametric analyses.

Figure 1 shows the drive and the damping rates regarding the sideband resonance of TAE with beam-ions with respect

**Table 1.** Normalized beam-ion orbit width for typical parameters in JET and KSTAR.  $\Delta_b/\Delta_m \lesssim 1$  for JET and KSTAR discharges with normal- $q_0$ , and  $\Delta_b/\Delta_m \gtrsim 1$  for KSTAR discharges with high- $q_0$ .

	JET	KSTAR with normal- $q_0$ ( $q_0 \sim 1$ )	KSTAR with high- $q_0$ ( $q_0 \sim 2$ )
Toroidal mode number, $n$	$\sim 5$	$\sim 3$	$\sim 3$
Local safety factor at $\rho_N \sim 0.5$ , $q$	$\sim 2$	$\sim 2$	$\sim 2.5$
NBI injected energy [keV]	$\sim 100$	$\sim 100$	$\sim 100$
Minor radius [m]	1	0.5	0.5
Toroidal magnetic field [T]	3.4	1.8	1.8
$\Delta_b/\Delta_m$	0.38 (damping-dominant)	0.86 (damping-dominant)	1.35 (drive-dominant)

**Figure 2.** Parametric scan of TAE stability by beam-ions with KSTAR discharges. The  $x$ -axis corresponds to the normalized beam-ion orbit width and the  $y$ -axis to the ratio of  $v_A$  to  $v_{0\parallel}$ . The colored contour indicates the normalized value of the linear growth rate by beam-ions, and the black dashed line the zero growth rate. The resonance condition between the TAE and beam-ions changes at the green horizontal line,  $v_A/v_{0\parallel} = |2s - 1|$ . The KSTAR discharges with and without TAE observation are shown with red and blue asterisk marks (and filled circles for #21695), respectively. In #21695, ECCD was applied to enhance the continuum damping by adjusting  $q$ -profile, which was not considered here. The typical ranges for the NBI in JET and ITER are also marked as circles.

to the normalized beam-ion orbit width by using the equations (2)–(4). Here, we assume  $v_{b0\parallel} \equiv v_0 \cos \theta_0 = v_A/3$ ,  $R/L_{pf} \equiv -R\beta'_b/\beta_b = 5$ , and  $\epsilon \equiv r/R = 0.1$ , which are typical values for the core region in present tokamaks. Mode drive by beam-ions increases linearly with  $\Delta_b/\Delta_m^{(o)}$  (or toroidal mode number as well) in the ZOW regime and decreases in the large-orbit regime, which is in agreement with [15, 26]. However, the orbit width dependence of the mode damping is different from that of the mode drive due to the relation (16). Mode damping by beam-ions is maximized in the ZOW regime and decreases faster than the mode drive in the large-orbit regime. Therefore, in the case of the sideband resonance of TAE with beam-ions, the drive is higher than the damping when  $\Delta_b/\Delta_m^{(o)} \gtrsim 1$  and vice versa when  $\Delta_b/\Delta_m^{(o)} \lesssim 1$  as shown in figure 1.

In JET, which shows beam damping of ICRH-driven TAE generally, one can check that  $\Delta_b/\Delta_m^{(o)} < 1$  (please refer to table 1) which is definitely located in the damping dominant region in figure 1. This is mainly due to the large size and magnetic field strength of JET which results in small  $\Delta_b/\Delta_m^{(o)}$ . In KSTAR, TAEs are often observed in high- $q_0$  (or  $q_{min}$ ) discharges such as high- $\beta_p$  scenarios [31], and rarely observed in low- $q_0$ 's even with the similar beam power. The dependence of  $q$  value on  $\Delta_b/\Delta_m^{(o)}$  ( $\propto q^2$ ) can give a clear explanation about these experimental tendencies as in table 1.

Since the parameters which can affect the beam-drive/damping of TAEs such as  $q$ ,  $v_A$ , and  $\omega_c$  are not significantly varying with radius in the core region, we can check the TAE stability with NBI only with OD parameters,  $q \simeq q_0$  and  $v_A \simeq B_0/\sqrt{\mu_0 \bar{n}_l M_i}$  where  $\bar{n}_l$  is the line-averaged density. We selected two dimensionless parameters  $v_A/v_{b0\parallel}$  and  $\Delta_b/\Delta_m^{(o)}$  which are mainly affecting equations (2)–(4). Then, we scanned those parameters of a set of discharges in KSTAR by using the measured OD parameters to evaluate the TAE stability, as shown in figure 2. Here,  $q_0$ 's are obtained from MSE-EFIT [32] (or EFIT [33] for the cases that MSE diagnostics are not available) and the line-averaged density  $\bar{n}_l$  from the interferometry [34, 35] or TRANSP-reconstruction [10, 36]. For simplicity, we assume  $R/L_{pf} = 5$ ,  $r/R = 0.17$ , and a birth pitch angle of beam-ions,  $\cos \theta_0 = 0.75$  which are typical values for  $r/a \lesssim 0.5$  region where the beam-pressure gradient is maximum. The KSTAR discharges selected for the analysis are listed in table 2.

Figure 2 shows a contour of the linear growth rate of TAE by beam-ions calculated by using the equations (2)–(4). The points for the KSTAR discharges are marked with red for the observed mode numbers of TAE and blue for mode numbers not observed (see table 2). The filled circles are from discharge #21695 where ECCD was applied to enhance the continuum damping by adjusting the  $q$ -profile [10], but this effect was not included here because the continuum damping is hard to be calculated precisely using OD parameters. The black dashed line indicates the zero growth rate, implying the balance between the mode drive and the damping by beam-ions. On the right side of the dashed line, the beam drive is dominant, and on the left side, beam damping is dominant. Discontinuities of the growth rate occur at the layers  $v_A/v_{0\parallel} = |2s - 1|$  (the green horizontal line in figure 2) because the resonance condition of the mode with beam-ions changes around those layers. Blue curves outside the upper and

**Table 2.** KSTAR discharges for the parametric analysis. The listed are the cases corresponding to the asterisk marks (and filled circles for #21695) in figure 2. TAEs were not observed in the second and last cases. In discharge #21695 (the last two cases),  $q$ -profile changes by ECCD after  $t = 5$  s [10].

Shot number	Time slice [s]	Observed toroidal mode number of TAE, $n$	EFIT type
#18597	8.0	2, 3, 4	EFIT
#18602	14.0	(Not observed)	EFIT
#21006	8.0	1, 2, 3	MSE-EFIT
#21693	8.0	2, 3, 4	MSE-EFIT
#21695	5.0	1, 2, 3	MSE-EFIT
#21695	8.0	(Not observed)	MSE-EFIT

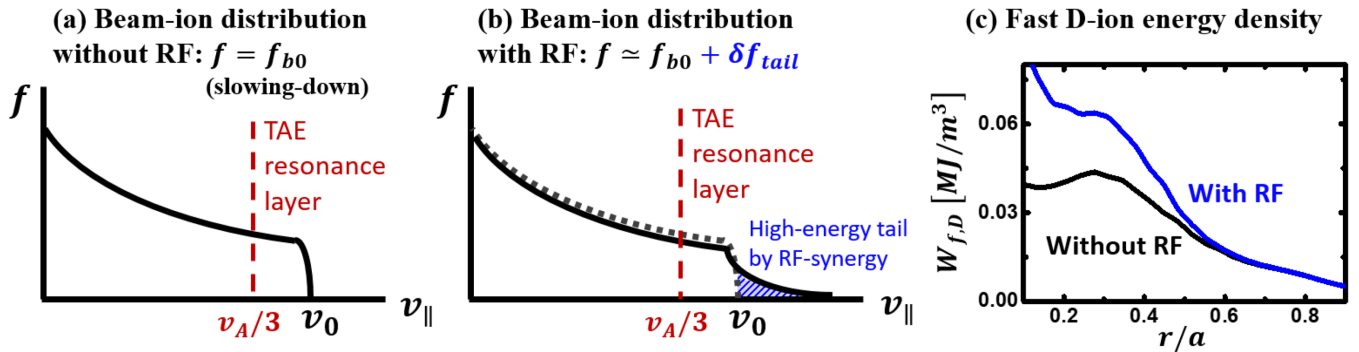


**Figure 3.** Velocity distribution function of beam-ions without (a) and with (b) considering RF-NB synergy effect. (c) The resulting variation of the beam-ion energy density profile calculated by PION-PENCIL. RF synergy effect generates the high-energy tail component,  $\delta f_{tail}$  (blue-shaded area in (b)). This high-energy tail part barely affects the interaction with TAEs due to its far distance from the resonance layer, but significantly enhance the beam energy density due to its high energy.

right sides of the figure show the change of the growth rate for each axis. In KSTAR, TAE interacts with beam-ions with the sideband resonance and the beam-destabilizing criterion well matches with the experimental observation. Since  $v_A/v_{b0||}$  is not significantly varying for given beam energy and operating scenarios, the normalized beam-ion orbit width  $\Delta_b/\Delta_m^{(o)}$  is the crucial parameter for determining the role of the beam-ions on TAE. Notably, this parameter is strongly affected by the local  $q$  value which can easily vary by external current drives such as ECCD or NBCD. For the cases included in this parametric scan, it was found that TAEs were more frequently observed in high- $q$  cases in KSTAR. Beam-stability regime for JET and ITER are also shown in figure 2. As discussed previously, JET parameters are seen to be obviously in the damping-dominant regime. On the other hand, NBI in ITER is expected to drive TAE much more than present devices due to its high energy ( $\sim 1$  MeV) satisfying the  $v_{||} = v_A$  resonance condition, whose mode drive is much stronger than that of the other sideband resonances.

#### 4. Application to linear stability analysis in a time-evolving JET plasma

In order to validate the model, we applied the formulas to a time-evolving JET deuterium plasma, discharge #92416 for linear stability analyses. In this discharge, ICRH was continuously applied to generate hydrogen-minority fast ions and to drive TAEs for predicting the energetic particle effect in future DT plasmas. NBI was initially injected with a relatively low

power and increased to stabilize TAEs, then turned off later to see the afterglow TAEs. Therefore, this discharge is highly suitable for validating the criterion and conditions for the mode drive by ICRH and damping by NBI that change over time. More information of this discharge can be found in [37].

##### 4.1. Modeling for the linear stability analysis of TAE with JINTRAC

JINTRAC [38] is a suite of codes for integrated simulations of tokamak scenarios, including various tokamak-physics modules such as a plasma transport code, JETTO [39] and external heating codes such as PION-PENCIL [40, 41]. For the computation of the linear stability of TAEs with JINTRAC, we use the magnetic equilibrium reconstructed by EFIT [33] with Faraday-constraint (EFTF), high-resolution Thomson scattering (HRTS) diagnostics for the electron density and temperature profiles [42], and the ion temperature profile reconstructed by TRANSP [36] as input profiles. PION-PENCIL codes compute the fast-ion-related profiles by NBI and ICRH from the given plasma profiles, then we can estimate the linear growth rate of TAE for the given toroidal mode number by using equation (1).

The PION-PENCIL integrated codes calculate fast ion quantities by NBI and ICRH, especially including the NB-RF synergy effect generating the high-energy tail component in the beam-ion distribution. Figures 3(a) and (b) describe the velocity distribution of beam-ions without and with considering NB-RF synergy effect, respectively. The high-energy tail part with  $v \gg v_0 \sim v_A/3$  barely affects the interaction with

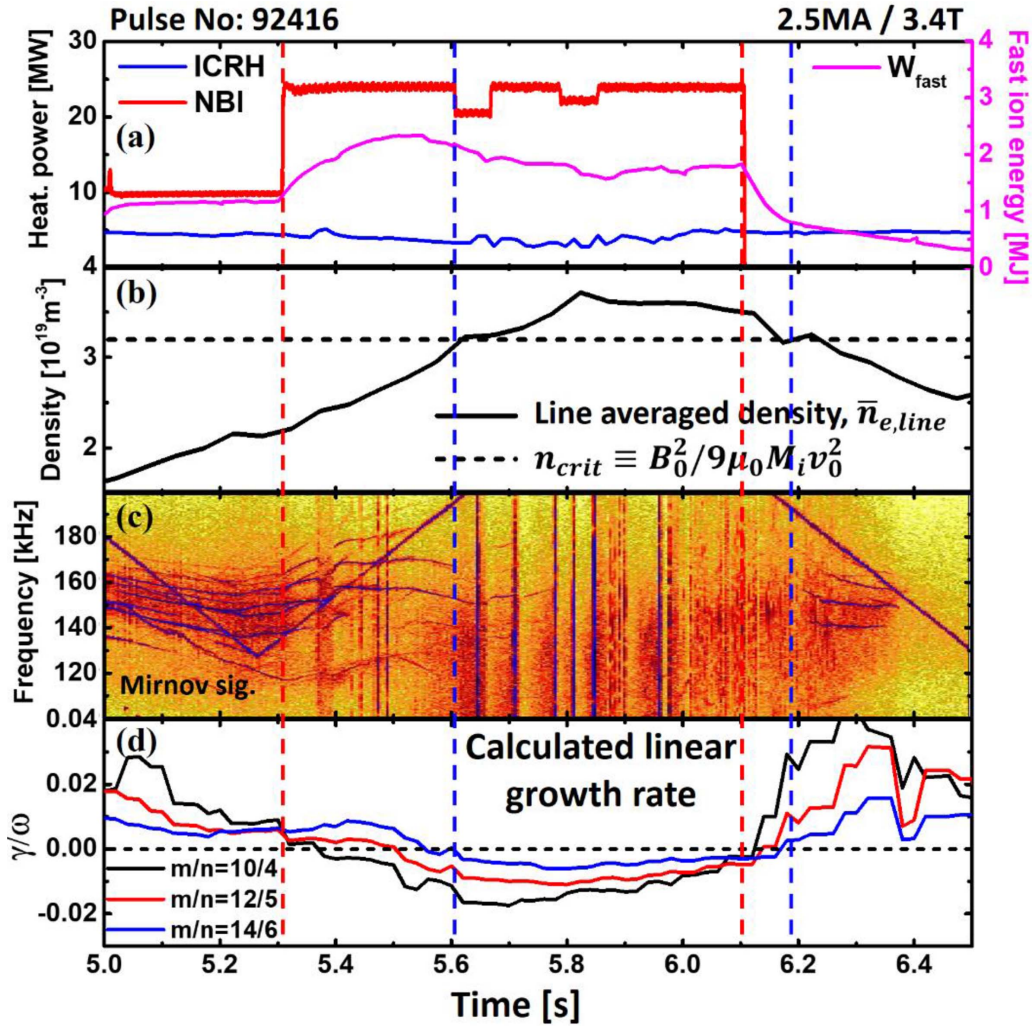


**Figure 4.** Time-evolution of heating power (a), line-averaged density (b), Mirnov signal of TAEs (c), and the calculated linear growth rates using analytic formulas (d). TAEs are initially derived by ICRH fast ions, then disappear at  $t \approx 5.6$  s by beam damping, and afterglow TAEs appear at  $t \approx 6.2$  s as beam power off.  $q_0$  is above 2.0 during this time domain.

TAEs due to its far distance from the resonance layer and low population. However, due to the high energy of the tail part, the NB-RF synergy effect can significantly enhance the energy density of the beam-ions even with its extremely low population as shown in figure 3(c). This enhancement of the beam energy density makes us overestimate the growth rate calculated by equations (2)–(4) which are assuming the beam distribution as a slowing-down distribution without considering the tail part. This overestimation comes from the fact that the interaction between beam-ions and TAEs depends on  $f_{v_{\parallel}=v_A/3}$  (and  $\partial f_{v_{\parallel}=v_A/3}/\partial r$ ) rather than  $\beta_b$  (and  $d\beta_b/dr$ ). Therefore, the RF contribution on the beam energy density was excluded intentionally with another PION run without RF power to avoid the unphysical results here.

#### 4.2. Time-evolution of linear stability of TAE in discharge #92416 on JET

The time-varying linear stability of TAEs in discharge #92416 is computed by using the formula,  $\frac{\gamma}{\omega}|_{n,m} \simeq \left(\frac{\gamma}{\omega}\right)_{NB} + \left(\frac{\gamma}{\omega}\right)_{RF} +$

$\left(\frac{\gamma}{\omega}\right)_i + \left(\frac{\gamma}{\omega}\right)_e$  with the JINTRAC suite of codes. The toroidal mode numbers of TAEs used in this analysis are  $n = 4, 5, 6$  which were estimated by the toroidal array of Mirnov coils [37].

Figure 4 shows the time-evolutions of the heating power and absorbed fast ion energy by NBI and ICRH, line-averaged density by HRTS, Mirnov signal of TAEs, and calculated linear growth rates using analytic formulas for discharge #92416. TAEs are initially driven by continuously injected ICRH as seen in figures 4(a) and (c). At  $t = 5.3$  s, the NBI power is increased from 10 MW to 25 MW, and the density gradually increases by the NBI fueling as shown in figure 4(b). As the line-averaged density exceeds a critical value  $n_{crit} \equiv B_0^2/9\mu_0 M_i v_0^2$  (black dashed line in figure 4(b)) eventually, beam-ions interact with TAEs, and then the modes disappear by the beam damping. This critical density is the minimum value to satisfy the beam-TAE resonance condition,  $v_0 \geq v_A/3$ .

In figure 4(a), we can see that the absorbed beam energy hits the maximum before  $t \approx 5.5$  s after the increase of the NBI power at  $t = 5.3$  s. This is consistent with the thermalization

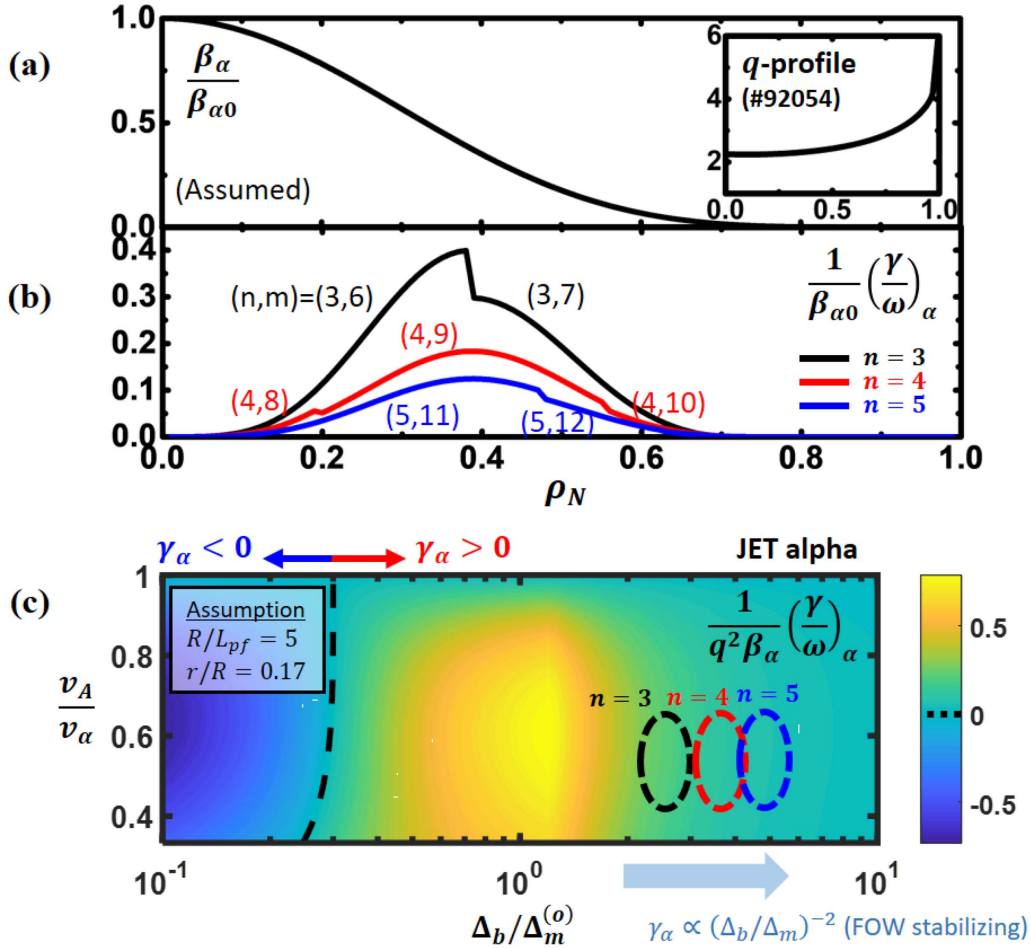


**Figure 5.** (a) The profiles of toroidal beta of alpha particles and  $q$ -profile for prediction of the TAE stability by alpha particles in JET DT plasmas. (b) The calculated linear growth rate by alpha particles for  $n = 3, 4$  and  $5$  modes using analytic formulas. The  $x$ -axis in (a) and (b) is the normalized toroidal magnetic flux,  $\rho_N$ . (c) The linear growth rate by alpha particles with respect to  $\Delta_b / \Delta_m^{(o)}$  and  $v_A / v_\alpha$ . The range for each mode number of TAE in JET DT plasmas is shown with the dashed circle.

time of beam-ions,  $\tau_{\text{th,b}} = \frac{\tau_{\text{sl}}}{3} \ln \left( \frac{v_0^3 + v_c^3}{v_c^3} \right) \sim 150$  ms. However, TAEs are still undamped over  $\sim 100$  ms after enough beam absorption, which indicates that the strong interaction of TAEs with the beam-ions occurs at a rather high density in JET to satisfy the resonance condition. As the beam power is turned off at  $t = 6.1$  s, the beam energy density and the plasma density are decreased again, and then afterglow TAEs reappear with diminishing beam damping. The red and the blue vertical dashed line show the time of NBI power change and the time satisfying the density criterion, respectively, where we can see that the TAE (dis-)appearance seems to be correlated with the density criterion as well as the absorbed beam energy.

Figure 4(d) shows the calculation of the linear growth rate from equation (1) for given mode numbers. Each term in equation (1) is obtained by using the analytic expressions shown in section 2. The toroidal mode numbers are chosen as  $n = 4, 5, 6$  which are the most unstable modes at  $t \approx 6.3$  s [37] and poloidal mode numbers as  $m = nq - 0.5$  around the most unstable region. In discharge #92416, the  $q$ -profile is quite flat in the core region, and the central value is varying in the range  $2.1 \lesssim q_0 \lesssim 2.3$  in the time domain shown in figure 4,

so  $(m/n) = (10/4, 12/5, 14/6)$  are used for the computation. Even though these analytic estimations have somewhat simple assumptions such as the slowing-down distribution for beam-ions and bi-Maxwellian for ICRH fast ions, it could reproduce the stability of TAE in various heating and density conditions in JET. Besides, this analysis allows a much faster estimation of the linear stability of TAEs than other simulations, highly desirable for the fast prediction or scenario development.

## 5. Prediction of alpha particle contribution to TAE for DT scenarios in JET

In JET, MeV-range hydrogen minority ions are created by ICRH in deuterium plasmas in order to probe the TAE instability threshold, to mimic the effect of alpha particles in DT plasmas in the upcoming JET DT campaign. However, we should note that the ICRH- and alpha-driven TAEs can be different due to different fast ion distributions and resonance mechanisms, as discussed in sections 2.1 and 2.2. In this section, we predict the alpha particle effect on the TAE stability in JET DT plasmas by using analytic formulas.

First, we chose discharge #92054 for the reference pulse, which uses only NBI heating at the peak performance time for a DT-relevant experiment. Then we assumed a core-peaked alpha particle pressure profile, and used the  $q$ -profile at  $t \approx 6.4$  s in discharge #92054, as shown in figure 5(a). Then we calculated the linear growth rates of  $n = 3, 4, 5$  TAEs by alpha particles by using equations (6)–(7) in figure 5(b). Here, we chose the toroidal mode numbers around  $n = 5$ , which is the most unstable mode number in ICRH-driven plasmas to compare the TAE drives by alpha particles and ICRH fast ions. As we expected, the  $(\gamma/\omega)_\alpha$  profile peaks near  $\rho_N \sim 0.4$  where the pressure gradient of alpha particles is maximized. In the previous prediction for DT plasmas in JET, the toroidal beta of alpha particles is estimated to be  $\beta_{\alpha 0} \sim 0.1\%$  [37]. In this situation, the linear growth rate by alpha particles  $(\gamma/\omega)_\alpha$  is  $O(10^{-4})$  from an estimation in figure 5(b), which is relatively low comparing with ICRH drive in deuterium plasmas ( $(\gamma/\omega)_{RF} = O(10^{-2})$  in figure 4(d)).

This relatively low alpha particle drive of TAEs is because of the finite-orbit-width stabilizing effect. The drift orbit width of 3.5 MeV alpha particles is much larger than the mode width. In this regime, the linear growth rate is proportional to  $(\Delta_b/\Delta_m^{(o)})^{-2}$ . Figure 5(c) indicates that  $n = (3 - 5)$  TAEs in JET DT plasmas (marked with dashed circles) are not significantly unstable by alpha particles, and rather lower  $n$  (resulting in lower  $\Delta_b/\Delta_m^{(o)}$ ) modes are more likely excited by them. However, for the low- $n$  ( $n \sim 1$ ) modes, damping effect by beam-ions (as shown in figure 1) and the interaction with the Alfvén continuum might also be significant. This result is consistent with that there were not clear observations of alpha-driven TAEs except the afterglow modes in the past DT campaign in JET [12].

## 6. Conclusions

A parametric analysis of TAE stability in the presence of beam-ions is conducted using analytic expressions which include the finite orbit width effects. It is found that the orbit width of the beam-ions normalized to the mode width,  $\Delta_b/\Delta_m$ , is a key parameter which quantifies the influence of NBI on the TAE stability. In the case of the sideband resonance of TAE with beam-ions, the mode drive is dominant for  $\Delta_b/\Delta_m \gtrsim 1$  and the damping is dominant for  $\Delta_b/\Delta_m \lesssim 1$ . This result could explain the beam damping effect of TAE commonly observed in JET and the reason why TAEs are more often observed in high- $q_0$  discharges in KSTAR. For analyses of the cases that the beam damps ICRH-driven TAEs in JET, the linear growth rate of TAE driven by ICRH fast ions is derived using a bi-Maxwellian distribution for the fast ion. Then, a linear stability analysis of TAEs in a time-varying plasma is performed for a JET discharge. We found that TAEs are excited by ICRH and then, damped as the beam beta increases and the plasma density exceeds a critical value for the resonance. It is noteworthy that the strong beam damping of TAE occurs only in plasmas with a rather high density so that  $v_A$  is low enough to satisfy the resonance condition  $v_{\parallel} = v_A/3$ . In JET plasmas with densities lower than this critical

value, the interaction of TAEs with the beam ions is turned out to be weak. The stability analysis using these analytic expressions successfully reproduced these experimental trends despite their simple assumptions. In addition, alpha particle effect on TAEs in JET predicted DT plasmas is estimated by using this model. The result indicates that alpha-driven TAEs are not significantly unstable compared to ICRH-driven TAEs. In this study, in order to focus on the particle interactions with TAEs, we chose the discharge with a flat  $q$ -profile which minimizes continuum and radiative damping of moderate- $n$  ( $n \sim 5$ ) TAEs. However, for high- $n$  TAEs with the finite magnetic shear and high temperature plasmas such as JET DT experiments and ITER, those damping processes could be important for the TAE stability due to its strong dependence on the mode number and the electron temperature. The method employed in this work can be used for extensive parametric studies at low computational cost, to help optimizing the scenarios being prepared for alpha-driven TAEs observations in JET DT.

## Acknowledgments

This work has been carried out within the framework of the EUROfusion Consortium and has received funding from the Euratom research and training programme 2014-2018 and 2019-2020 under Grant Agreement No. 633053. The views and opinions expressed herein do not necessarily reflect those of the European Commission. Authors would like to express our gratitude to The Research Institute of Energy and Resources and The Institute of Engineering Research at Seoul National University. This research was supported by R&D Program No. CN1901 through the National Fusion Research Institute of Korea (NFRI) funded by the Government funds. This work was supported by National R&D Program through the National Research Foundation of Korea(NRF) funded by the Ministry of Science & ICT (NRF-2019M1A7A1A03089798).

## ORCID iDs

J. Seo  <https://orcid.org/0000-0003-0635-0282>

J. Kim  <https://orcid.org/0000-0001-7792-3581>

R.J. Dumont  <https://orcid.org/0000-0002-1030-138X>

F.J. Casson  <https://orcid.org/0000-0001-5371-5876>

## References

- [1] Cheng C.Z., Chen L. and Chance M.S. 1985 High- $n$  ideal and resistive shear Alfvén waves in tokamaks *Ann. Phys.* **161** 21–47
- [2] Cheng C.Z. and Chance M.S. 1986 Low- $n$  shear Alfvén spectra in axisymmetric toroidal plasmas *Phys. Fluids* **29** 3695–701
- [3] Rosenbluth M.N. and Rutherford P.H. 1975 Excitation of Alfvén waves by high-energy ions in a tokamak *Phys. Rev. Lett.* **34** 1428
- [4] Zhu Y.B., Heidbrink W.W. and Pickering L.D. 2010 Phenomenology of energetic-ion loss from the DIII-D tokamak *Nucl. Fusion* **50** 084024
- [5] Zweben S.J., Darrow D.S., Fredrickson E.D., Taylor G., Von Goeler S. and White R.B. 1999 MHD induced alpha particle loss in TFTR *Nucl. Fusion* **39** 1097

- [6] Pinches S.D. et al 2006 Observation and modelling of fast ion in JET and ASDEX upgrade *Nucl. Fusion* **46** S904
- [7] Kiptily V.G. et al 2009 Recent progress in fast ion studies on JET *Nucl. Fusion* **49** 065030
- [8] García-Muñoz M. et al 2009 MHD induced fast-ion losses on ASDEX Upgrade *Nucl. Fusion* **49** 085014
- [9] Kim J. et al 2018 Experimental observations of beam-driven Alfvén eigenmodes in KSTAR *Preprint: 2016 IAEA Fusion Energy Conf.* (Kyoto, Japan, 17–22 October 2016) EX/P4-26 (<https://nucl.iaea.org/sites/fusionportal/Shared%20Documents/FEC%202016/fec2016-preprints/preprint0773.pdf>)
- [10] Kim J. et al 2019 Suppression of toroidal Alfvén eigenmodes by the electron cyclotron current drive in KSTAR plasmas *16th IAEA Technical Meeting on Energetic Particles in Magnetic Confinement Systems—Theory of Plasma Instabilities (Shizuoka, Japan)* P1–2 (<https://conferences.iaea.org/event/185/contributions/14984/attachments/8122/10738/49-Kim.pdf>)
- [11] Fu G.Y., Cheng C.Z., Budny R., Chang Z., Darrow D.S., Fredrickson E., Mazzucato E., Nazikian R., Wong K.L. and Zweben S. 1996 Analysis of alpha particle-driven toroidal Alfvén eigenmodes in Tokamak Fusion Test Reactor deuterium–tritium experiments *Phys. Plasmas* **3** 4036–45
- [12] Sharapov S.E., Borba D., Fasoli A., Kerner W., Eriksson L.G., Heeter R.F., Huysmans G.T.A. and Mantsinen M.J. 1999 Stability of alpha particle driven Alfvén eigenmodes in high performance JET DT plasmas *Nucl. Fusion* **39** 373
- [13] Fu G.Y. and Van Dam J.W. 1989 Excitation of the toroidicity-induced shear Alfvén eigenmode by fusion alpha particles in an ignited tokamak *Phys. Fluids B* **1** 1949–52
- [14] Berk H.L., Breizman B.N. and Ye H. 1992 Finite orbit energetic particle linear response to toroidal Alfvén eigenmodes *Phys. Lett. A* **162** 475–81
- [15] Breizman B.N. and Sharapov S.E. 1995 Energetic particle drive for toroidicity-induced Alfvén eigenmodes and kinetic toroidicity-induced Alfvén eigenmodes in a low-shear tokamak *Plasma Phys. Control. Fusion* **37** 1057
- [16] Fülöp T., Lisak M., Kolesnichenko Y.I. and Anderson D. 1996 Finite orbit width stabilizing effect on toroidal Alfvén eigenmodes excited by passing and trapped energetic ions *Plasma Phys. Control. Fusion* **38** 811–28
- [17] Rosenbluth M.N., Berk H.L., Van Dam J.W. and Lindberg D.M. 1992 Continuum damping of high-mode-number toroidal Alfvén waves *Phys. Rev. Lett.* **68** 596
- [18] Zonca F. and Chen L. 1992 Resonant damping of toroidicity-induced shear-Alfvén eigenmodes in tokamaks *Phys. Rev. Lett.* **68** 592
- [19] Mett R.R. and Mahajan S.M. 1992 Kinetic theory of toroidicity-induced Alfvén eigenmodes *Phys. Fluids B* **4** 2885–93
- [20] Gorelenkov N.N., Berk H.L., Budny R., Cheng C.Z., Fu G.Y., Heidbrink W.W., Kramer G.J., Meade D. and Nazikian R. 2003 Study of thermonuclear Alfvén instabilities in next step burning plasma proposals *Nucl. Fusion* **43** 594
- [21] Pinches S.D., Chapman I.T., Lauber P.W., Oliver H.J.C., Sharapov S.E., Shinohara K. and Tani K. 2015 Energetic ions in ITER plasmas *Phys. Plasmas* **22** 021807
- [22] Ghantous K., Gorelenkov N.N., Berk H.L., Heidbrink W.W. and Van Zeeland M.A. 2012 1.5D quasilinear model and its application on beams interacting with Alfvén eigenmodes in DIII-D *Phys. Plasmas* **19** 092511
- [23] Betti R. and Freidberg J.P. 1992 Stability of Alfvén gap modes in burning plasmas *Phys. Fluids B* **4** 1465–74
- [24] Chang C.S. and Colestock P. 1990 Anisotropic distribution function of minority tail ions generated by strong ion cyclotron resonance heating *Phys. Fluids B* **2** 310
- [25] Gorelenkov N.N. and Sharapov S.E. 1992 On the collisional damping of TAE-modes on trapped electrons in tokamaks *Phys. Scr.* **45** 163
- [26] Fu G.Y. and Cheng C.Z. 1992 Excitation of high-n toroidicity-induced shear Alfvén eigenmodes by energetic particles and fusion alpha particles in tokamaks *Phys. Fluids B* **4** 3722–34
- [27] Berk H.L. and Breizman B.N. 1990 Saturation of a single mode driven by an energetic injected beam. III. Alfvén wave problem *Phys. Fluids B* **2** 2246–52
- [28] Hahn T.S. and Chen L. 1995 Nonlinear saturation of toroidal Alfvén eigenmodes via ion Compton scattering *Phys. Rev. Lett.* **74** 266
- [29] Qiu Z., Chen L. and Zonca F. 2019 Gyrokinetic theory of the nonlinear saturation of a toroidal Alfvén eigenmode *Nucl. Fusion* **59** 066024
- [30] Qiu Z., Chen L., Zonca F. and Chen W. 2019 Nonlinear excitation of a geodesic acoustic mode by toroidal Alfvén eigenmodes and the impact on plasma performance *Nucl. Fusion* **59** 066031
- [31] Kang J.S. et al 2019 Role of fast-ion transport to sustain the high q min profile in KSTAR discharges *16th IAEA Technical Meeting on Energetic Particles in Magnetic Confinement Systems—Theory of Plasma Instabilities (Shizuoka, Japan)* P1–17 ([https://conferences.iaea.org/event/185/contributions/14967/attachments/8087/10661/EPPI2019\\_jskang\\_A0.pdf](https://conferences.iaea.org/event/185/contributions/14967/attachments/8087/10661/EPPI2019_jskang_A0.pdf))
- [32] Levinton F.M., Fonck R.J., Gammel G.M., Kaita R., Kugel H.W., Powell E.T. and Roberts D.W. 1989 Magnetic field pitch-angle measurements in the PBX-M tokamak using the motional Stark effect *Phys. Rev. Lett.* **63** 2060
- [33] Lao L.L., Ferron J.R., Groebner R.J., Howl W., St. John H., Strait E.J. and Taylor T.S. 1990 Equilibrium analysis of current profiles in tokamaks *Nucl. Fusion* **30** 1035
- [34] Nam Y.U., Cheon M.S., Kwon M. and Hwang Y.S. 2003 Design of a single-channel millimeter-wave interferometer system for Korea superconducting tokamak advanced research *Rev. Sci. Instrum.* **74** 1613–16
- [35] Lee K.C., Juhn J.W., Nam Y.U., Kim Y.S., Wi H.M., Kim S.W. and Ghim Y.C. 2016 The design of two color interferometer system for the 3-dimensional analysis of plasma density evolution on KSTAR *Fusion Eng. Des.* **113** 87–91
- [36] Goldston R.J., McCune D.C., Towner H.H., Davis S.L., Hawryluk R.J. and Schmidt G.L. 1981 New techniques for calculating heat and particle source rates due to neutral beam injection in axisymmetric tokamaks *J. Comput. Phys.* **43** 61–78
- [37] Dumont R.J. et al 2018 Scenario development for the observation of alpha-driven instabilities in JET DT plasmas *Nucl. Fusion* **58** 082005
- [38] Romanelli M. et al 2014 JINTRAC: a system of codes for integrated simulation of tokamak scenarios *Plasma Fusion Res.* **9** 3403023
- [39] Cenacchi G. and Taroni A. 1988 JETTO: a free-boundary plasma transport code (basic version) report JET-IR (88) 03 JET joint undertaking JET Team
- [40] Challis C.D., Cordey J.G., Hamnén H., Stubberfield P.M., Christiansen J.P., Lazzaro E., Muir D.G., Stork D. and Thompson E. 1989 Non-inductively driven currents in JET *Nucl. Fusion* **29** 563
- [41] Eriksson L.G., Hellsten T. and Willen U. 1993 Comparison of time dependent simulations with experiments in ion cyclotron heated plasmas *Nucl. Fusion* **33** 1037
- [42] Pasqualotto R., Nielsen P., Gowers C., Beurskens M., Kempnaars M., Carlstrom T. and Johnson D. 2004 High resolution Thomson scattering for Joint European Torus (JET) *Rev. Sci. Instrum.* **75** 3891
- [43] Joffrin E.H. et al 2019 Overview of the JET preparation for deuterium–tritium operation with the ITER like-wall *Nucl. Fusion* **59** 112021